Articles

Three-Dimensional Structure of Human Adenine Phosphoribosyltransferase and Its Relation to DHA-Urolithiasis[†,‡]

Marcio Silva,[§,||] Carlos Henrique Tomich de Paula Silva,[§,||,⊥] Jorge Iulek,[#] and Otavio Henrique Thiemann*[,§]

Laboratory of Protein Crystallography and Structural Biology, Physics Institute of São Carlos, University of São Paulo, Av. Trabalhador Sãocarlense 400, P.O. Box 369, 13566-590 São Carlos, SP, Brazil, and Department of Chemistry, Biotechnology Center, State University of Ponta Grossa, PR, Brazil

Received November 19, 2003; Revised Manuscript Received April 14, 2004

ABSTRACT: In mammals, adenine phosphoribosyltransferase (APRT, EC 2.4.2.7) is present in all tissues and provides the only known mechanism for the metabolic salvage of adenine resulting from the polyamine biosynthesis pathway or from dietary sources. In humans, APRT deficiency results in serious kidney illness such as nephrolithiasis, interstitial nephritis, and chronic renal failure as a result of 2,8-dihydroxyadenine (DHA) precipitation in the renal interstitium. To address the molecular basis of DHA-urolithiasis, the recombinant human APRT was crystallized in complex with adenosine 5′-monophosphate (AMP). Refinement of X-ray diffraction data extended to 2.1 Å resolution led to a final crystallographic R_{factor} of 13.3% and an R_{free} of 17.6%. This structure is composed of nine β-strands and six α-helices, and the active site pocket opens slightly to accommodate the AMP product. The core of APRT is similar to that of other phosphoribosyltransferases (PRTases), although the adenine-binding domain is quite different. Structural comparisons between the human APRT and other "type I" PRTases of known structure revealed several important features of the biochemistry of PRTases. We propose that the residues located at positions corresponding to Leu159 and Ala131 in hAPRT are responsible for the base specificities of type I PRTases. The comparative analysis shown here also provides structural information for the mechanism by which mutations in the human APRT lead to DHA-urolithiasis.

Usually, adenine is detected at low levels in blood and urine due to APRT activity (*1*, *2*). In mammals, adenine phosphoribosyltransferase (APRT)[1] is present in all tissues and provides the only known mechanism for the metabolic salvage of adenine resulting from the polyamine biosynthesis pathway or from dietary sources (*3*−*5*). Two types of deficiencies are currently recognized in humans, both due to mutations in the APRT gene. Type I deficiency is the result of a complete loss of APRT activity (*5*), whereas in type II deficiency, APRT has a reduced affinity for PPRP, leading to a 10-fold increase in the K_m for this substrate (*6*). Both types of deficiency result in the accumulation of adenine, which is then oxidized by xanthine dehydrogenase (XDH, EC 1.2.3.2) to 2,8-dihydroxyadenine (DHA), via an 8-hydroxyadenine intermediate (*7*). DHA either is eliminated through the urine or, in large amounts, can precipitate in the kidney tubules due to its low solubility, resulting in 2,8-dihydroxyadenine stones and urolithiasis (*8*). The major clinical manifestations associated with APRT deficiency-related kidney diseases are the appearance of kidney stones, crystalluria, hematuria, dysuria, and infections in the urinary tract (*8*). Such a clinical profile can result in severe kidney failure.

Phosphoribosyltransferases (PRTases) catalyze the displacement of a PRPP α-1′-pyrophosphate through a nitrogen-containing nucleophile. The reaction products are a β-1-substituted ribose 5′-phosphate and a free pyrophosphate (PP) (*9*). The nucleophile for most PRTases is a nucleotide base, while the product is a nucleoside 5′-monophosphate. The proposed nucleophilic attack by the purine or pyrimidine base at the PRPP ribose C1′ atom involves a sequential process

[†] This work was supported in part by Grant 99/02874-9 (FAPESP) and received financial support from the UNDP/World Bank/WHO Special Programme for Research and Training in Tropical Diseases (TDR) (to O.H.T.). M.S. and C.H.T.d.P.S. are FAPESP fellowship awardees. This work has been partially supported by the National Synchrotron Light Laboratory (LNLS), Brazil, Proposal 1237/02, for the data collection at the Protein Crystallography Beamline.

[‡] Coordinates for the human APRT X-ray structure have been deposited in the Protein Data Bank (entry 1ORE).

* To whom correspondence should be addressed. Phone: (55-16) 273-8089. Fax: (55-16) 273-9881. E-mail: thiemann@if.sc.usp.br.

[§] University of São Paulo.

[||] These authors contributed equally to this work.

[⊥] Current address: School of Pharmaceutical Sciences of Ribeirão Preto, University of São Paulo, Av. do Café, s/n, 14040-903 Ribeirão Preto, SP, Brazil.

[#] State University of Ponta Grossa.

[1] Abbreviations: APRT, adenine phosphoribosyltransferase; PRTase, phosphoribosyltransferase; hAPRT, human adenine phosphoribosyltransferase; IPTG, isopropyl β-D-1-thiogalactopyranoside; 3D, three-dimensional; AMP, adenosine monophosphate; Tris, tris(hydroxymethyl)-aminomethane; SDS−PAGE, sodium dodecyl sulfate−polyacrylamide gel electrophoresis; PRPP, phosphoribosylpyrophosphate; PP, pyrophosphate.

10.1021/bi0360758 CCC: $27.50
Published on Web 05/25/2004

during which pyrophosphate is released first, followed by the release of the nucleoside product, in either an S_N1 or S_N2 displacement mechanism (*10*). If the reaction occurs by an S_N1-type mechanism of nucleophilic displacement, one transition state is supposed to involve a positively charged oxycarbonium molecule. On the other hand, in an S_N2-type nucleophilic displacement, the enzyme would promote simultaneous nucleophilic attack and product formation, where a rapid PRPP transfer is thought to take place with the formation of a ternary complex (*11*).

PRTases are classified into two groups named type I and type II. The type I PRTases are structurally identified by a conserved PRPP binding motif, which features two adjacent acidic residues surrounded by one or more hydrophobic residues (*12*). These PRTases reveal a common α/β-fold at the PRPP binding motif and a flexible loop, besides a core region of at least five parallel β-strands surrounded by three or more α-helices (*9, 12*). Type I PRTases present also a structurally variable region, called the hood subdomain, which is implicated in the base specificity (*9, 12*). At present, the *Salmonella typhimurium* quinolinate phosphoribosyltransferase (QPRT) is the only known structure of a "type II" PRTase. This PRTase does not present a PRPP binding motif and is composed of a mixed α/β N-terminal domain and an α/β barrel-like C-terminal domain (*13*).

The human APRT (hAPRT) structure reported in this work represents the first mammalian type I APRT crystallized with its structure resolved. Moreover, this work provides new information: the identification of the residues responsible for the adenine specificity through the comparison of this structure with other known PRTase structures and the structural basis for the serious clinical dysfunction known as urothialisis resulting from APRT mutations. This represents a fundamental contribution to the understanding of the catalytic mechanism as well as of the role of the APRT mutations associated with human disease.

MATERIALS AND METHODS

Human aprt PCR Cloning and Expression. The *haprt* gene was amplified from a human fetal brain cDNA library (Invitrogen) by the polymerase chain reaction (PCR) based on the available sequence (GenBank accession number NM_000485.1). Two oligodeoxynucleotide primers for PCR amplification, with *Nde*I and *Xho*I restriction sites introduced at the 5′ and 3′ ends, respectively [5′-GCACGCGCATATG-GCCGACTCCGAGCTGCA-3′ (*Nde*I) and 5′-AGGCTC-GAGGGTCACTCATACTGCAGGAG-3′ (*Xho*I)], were synthesized for insertion into the pET29a(+) expression vector (Novagen). The PCR, including 100 pmol of each primer and approximately 50 ng of the cDNA, was carried out in a GeneAmp 2400 thermocycler (Perkin-Elmer CETUS) with 5 units of AmpliTaq DNA polymerase (Promega), according to the manufacturer's instructions. The sample was initially subjected to a denaturation step at 367 K for 2 min, followed by 25 cycles of denaturation at 367 K for 0.5 min, then an annealing step at 313 K for 1.0 min, and an extension step at 345 K for 1 min. A DNA band of approximately 550 bp in length was gel purified by the NaI glass powder method (*14*). This purified DNA was then inserted into the pGEM-T vector (Promega) according to the manufacturer's instructions, and the vector thus prepared was used to transform *Escherichia coli* DH5α competent cells. The recombinant plasmid was purified by the alkaline lysis method (*15*) and the *haprt* gene sequence analyzed by sequencing in an ABI377 DNA sequencer to confirm the lack of PCR-introduced mutations. A selected clone was digested by the restriction enzymes *Nde*I and *Xho*I and the *haprt* gene inserted into the pET29a(+) vector and used to transform *E. coli* BL21(DE3) competent cells. Cells from a single colony were grown overnight at 310 K and 250 rpm in 5 mL of LB medium containing 30 μg/mL kanamycin. A larger cell culture was grown in 2xYT medium with 30 μg/mL kanamycin at 310 K and 250 rpm until an OD of 0.60 at 600 nm was reached. The culture was then induced for 6 h with 0.1 mM IPTG (final concentration).

Protein Purification. The recombinant hAPRT protein was obtained by a two-step purification protocol. All steps were carried out in ice unless otherwise indicated. The *E. coli* BL21(DE3) cell culture containing recombinant hAPRT was harvested by centrifugation at 6000*g* for 10 min. The cell pellet was suspended in 10 mL of 20 mM Tris-HCl (pH 7.4) and 5 mM $MgCl_2$ (buffer A), and cell lysis was performed on ice by sonication for 5 min (Fisher Scientific model 550 sonic dismembrator) at 1 min pulses with 1 min cooling. The crude extract was clarified by centrifugation at 20000*g* for 30 min. The clarified soluble fraction was then loaded onto a 10 mL N-6 attached AMP agarose column (SIGMA A3019), previously equilibrated with buffer A. The column was washed with the same buffer A (total volume of 40 mL) at a flow rate of 0.7 mL/min, and hAPRT was removed with 20 mL of buffer B (buffer A with 2 mM AMP). This partially purified hAPRT was further purified in a 25 mL Superose-12 column (Pharmacia Biotech), previously equilibrated with buffer A at a flow rate of 0.5 mL/min.

Protein Characterization. The apparent molecular mass of the protein under nondenaturing conditions was determined by analytical chromatography on a Superose 12 column (Pharmacia Biotech) as described. The isoelectric point for the recombinant hAPRT was determined by gel isoelectric focusing in a PHAST system (Pharmacia Biotech). The N-terminal amino acid sequence was determined subsequently by an automated Edman degradation method.

Enzymatic Assay. The PRPP and adenine K_m values were measured by the method described by Joel *et al*. (*16*) at 295 K using a reaction volume of 500 μL. The reaction was initiated by the addition of 20 nM recombinant hAPRT and monitored at 259 nm for 30 s. To determine the K_m for PRPP, the reaction mixture was supplemented with 50 μM adenine and the PRPP concentration was varied from 2.5 to 80 μM. To determine the K_m value for adenine, the reaction mixture was supplemented with 25 μM PRPP and the adenine concentration was varied from 1 to 10 μM.

Protein Crystallization, Diffraction Data Collection, and Processing. For the crystallization assays, performed at 291 K, the purified hAPRT was concentrated by ultrafiltration, using Centriprep and Centricon 10 concentrators (Millipore), up to 6 mg/mL in buffer B. Crystallization drops, by the hanging drop vapor diffusion method, were prepared by mixing 5 μL of the concentrated hAPRT with 5 μL of the crystallization solution. The crystallization solution was composed of 15.0% (v/v) glycerol, 25.5% (w/v) polyethylene glycol 4000, 0.17 mol/L sodium acetate, and 0.085 mol/L Tris-HCl (pH 8.5) in a volume of 500 μL. Small crystals

Table 1: Crystallographic Summary

Diffraction Data	
space group	$P4_32_12$
unit cell parameters *a* and *c* (Å)	58.31 and 109.54
resolution (Å)	40.0−2.10
no. of observed reflections	95875
no. of unique reflections	11527
refined mosaicity (deg)	0.307
overall completeness of data (%)	99.3
completeness in the last shell (2.22−2.10 Å) (%)	97.0
overall R_{merge} (%)	4.0
R_{merge} in the last shell (2.22−2.10 Å) (%)	11.2
overall $I/\sigma(I)$	12.2
Structure Refinement	
residues in most favored regions (%)	94.0
residues in additional allowed regions (%)	4.7
residues in generously allowed regions (%)	1.3
residues in disallowed regions (%)	0.0
overall R_{cryst} (%)	13.3
overall R_{free} (%)	17.6
high-resolution bin R_{cryst} (2.156−2.102 Å) (%)	13.4
high-resolution bin R_{free} (2.156−2.102 Å) (%)	25.7
rms deviations from ideal values, bond lengths (Å)	0.016
rms deviations from ideal values, bond angles (deg)	1.618

could be observed after 5 days, and reached a maximum size of 0.2 mm × 0.15 mm × 0.2 mm after 4 weeks. For data collection, single crystals were mounted on nylon loops (Hampton Research) and quickly frozen in a gaseous nitrogen flow at ~100 K (Oxford Cryosystems). Seventy sequential images, with an oscillation angle of 1° each, were recorded on a 345 MAR Research image plate detector at the National Laboratory for Synchrotron Light (LNLS-Campinas) with a wavelength of 1.4538 Å and a crystal to detector distance of 200 mm. The frames were processed using MOSFLM (*17*) and SCALA from the CCP4 package (*18*). General statistics are given in Table 1.

Initial Phasing, Model Building, and Refinement. Initial phasing was achieved by molecular replacement using AMoRe (*19*) and the *Leishmania tarentolae* APRT structure as the search model (*20*), from which the ligands and water molecules were excluded. The searches for the rotation and translation solutions were performed using data in the resolution range of 18.3−2.1 Å, which included 11 502 unique reflections. To minimize model bias, simulated annealing using the maximum likelihood method was performed, followed by coordinate and *B* factor refinement with data between 30.0 and 2.1 Å resolution, using CNS (*21*). The model was finally refined using REFMAC (*22*), including TLS parameters. During each refinement cycle, the model and the electron density maps were built with XFIT (*23*) and visually inspected. The remaining side chains were located by fitting the $2m|F_o| - D|F_c|$ electron density map, as calculated by REFMAC. Arp_waters (*24*) was used to locate water molecules based on both $2m|F_o| - D|F_c|$ and $m|F_o| - D|F_c|$ maps. Refinement was concluded when no significant changes in $R_{crystal}$ and R_{free} were observed and no more structured atoms could be added to the model.

PRTase Structural Comparisons. The refined human APRT structure was compared to other available phosphoribosyltransferase structures: *L. tarentolae* (PDB entry 1MZV), *Leishmania donovani* (PDB entries 1QB7, 1QB8, 1QCC, and 1QCD), *Saccharomyces cerevisiae* (PDB entries 1G2P and 1G2Q), *Giardia lamblia* APRT (PDB entries 1L1Q and 1L1R), *Toxoplasma gondii* UPRT (PDB entry 1BD4), *E. coli* XPRT (PDB entries 1A95, 1A96, 1A97, and 1A98) and OPRT (PDB entry 1ORO), *S. typhimurium* OPRT (PDB entries 1OPR and 1STO), *Trypanosoma cruzi* HGPRT (PDB entry 1TC2), *Homo sapiens* HGPRT (PDB entries 1HMP, 1BZY, and 1D6N), *Trichomonas foetus* HGXPRT (PDB entry 1HGX), and *T. gondii* HGXPRT (PDB entries 1DBR, 1FSG, 1QK3, 1QK4, and 1QK5). All structures were sequentially superimposed on the basis of the C_α coordinates of the "PRPP loop" (residues 147−151 of the human APRT), which is a structural motif characteristic of the PRTase family (*11*), and then visualized with O (*25*). Structures containing AMP bound were also superimposed with our structure on the basis of the C_α coordinates of the respective overall structures (Table 1).

RESULTS AND DISCUSSION

Characterization of the Recombinant Human APRT. The expression and purification protocol described here allowed the recovery of approximately 16 mg of pure recombinant hAPRT enzyme from 1 L of *E. coli* culture. After purification, activity assays and SDS−PAGE were used to monitor the purity of the sample. Via 15% SDS−PAGE, the purified recombinant hAPRT migrated as a single band at approximately 25 kDa. The apparent molecular mass determined by size-exclusion chromatography was 46 kDa, consistent with the proposed functional homodimer structure for the native human APRT. The N-terminal sequence of the recombinant protein was determined (ADSELQLVEQRI), and further model building of almost all residues onto the electron density map reinforced the identity with the native protein. The isoelectric point determined for the recombinant hAPRT was 5.4, close to the theoretical one of 5.8, as calculated with ProtParam using the amino acid sequence (*26*) and the values of 4.78 and 4.55 previously reported (*27*, *28*). K_m values for adenine and PRPP of 4 and 8.9 μM, respectively, were obtained, consistent with those reported for other mammalian APRT (*28*, *29*), and confirm the activity of the purified recombinant hAPRT.

Structure Determination. Crystals of the recombinant hAPRT protein belonged to the tetragonal system in space group $P4_32_12$ with the following cell parameters: $a = b =$ 58.31 Å and $c =$ 109.54 Å. X-ray diffraction data were processed up to 2.1 Å resolution and data collection statistics are presented in Table 1. Molecular replacement trials with AMoRe using the *L. tarentolae* APRT monomer resulted in a clear rotation and translation solution, confirming the $P4_32_12$ space group, with a correlation coefficient equal to 19.6%. The final refined hAPRT model comprises 179 amino acid residues (numbered 2−180), 206 water molecules, one AMP molecule, and one chloride ion per monomer. In general, the electron density for most of the structure, as well as for both ligands, was clearly interpretable (Figure 1). During structure building, residues 2 and 3 could be modeled with difficulty. Methionine 1 was excised during expression in *E. coli*.

Almost all residues are in either the most favored or favored regions of the Ramachandran plot. It is well-known that a magnesium ion plays an important role in the catalytic mechanism of PRTases (*9*). To analyze the presence of the magnesium ion, several searches using WASP (*30*) and Xpand (*31*) were performed. No single site for a Mg^{2+},

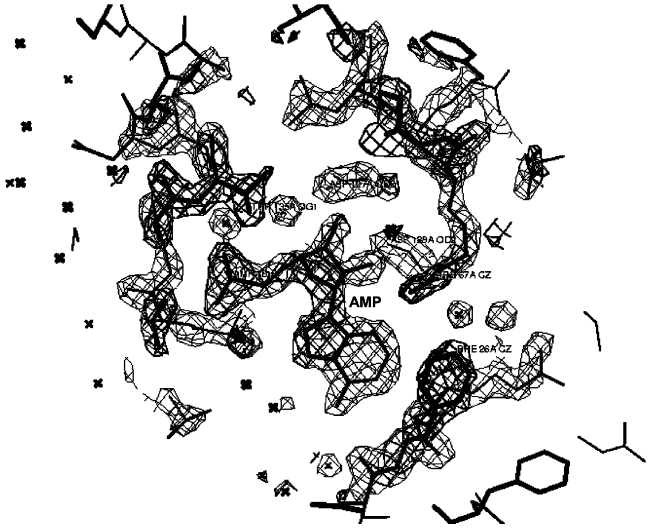

FIGURE 1: Electron density map at the active site showing the position of the bound AMP. A $2|F_o| - |F_c|$ omit map at 2.1 Å is shown phased with the final model at a contour level of 2.0σ. The bound AMP is identified. This figure was produced with Xfit.

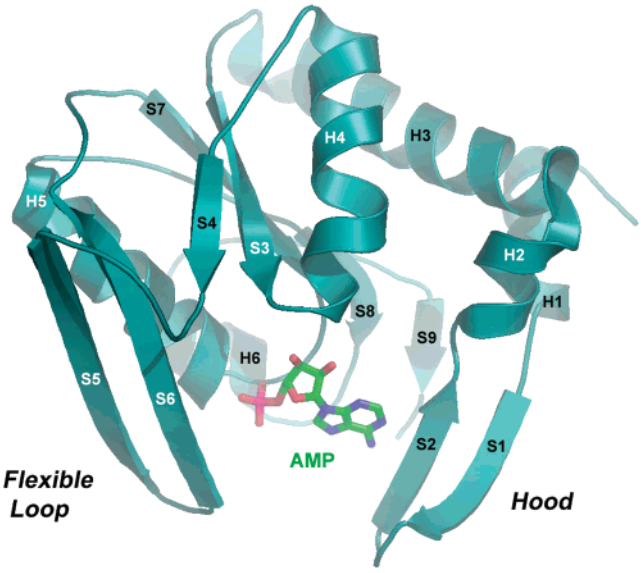

FIGURE 2: Ribbon diagram of the AMP-bound hAPRT monomer. The flexible loop, which is reported to sequester the substrates from the solvent, is shown in its open conformation. It is possible to visualize that it does not interact with the hood subdomain, which is important for base recognition.

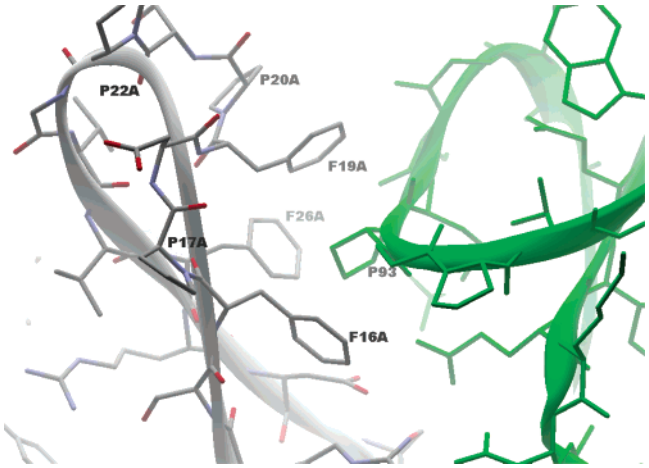

FIGURE 3: Calyx-like structural feature of the human APRT. Proline 93 (P93) belongs to the hAPRT dimer counterpart shown in green. The structural arrangement in the format of a calyx is formed by F19, F26, and F16 of one monomer (shown in gray) of the dimer arrangement. This figure was produced with Xfit.

complying with the minimum requisites of coordination and distances, could be found; therefore, the final structure is considered without the ion. On the other hand, electron density and surrounding atoms suggested the presence of a chloride ion near R87, with partial occupancy. Attempts were made to refine a water molecule in this position or an alternative conformation for the R87 side chain. Both led to poorer results in R_{factor} values and electron density, confirming our initial model with the chloride ion.

Overall Structure. The sequence and structure of hAPRT were somewhat identical to those of other known AMP-containing APRTs. The sequence of hAPRT is 44.7% identical to that of *S. cerevisiae* (PDB entry 1G2P), 36.6% identical to that of *G. lamblia* (PDB entry 1L1Q), and 27.5% identical to that of *Leishmania* (PDB entries 1MZV and 1QB7). The overall superposition of the hAPRT structure with the *Leishmania* AMP-containing APRTases revealed an rms of 1.25 Å. The human APRT is composed of nine β-strands and six α-helices, and can be divided into the "core" (residues 33−169), "hood" (residues 5−34), and "flexible loop" (residues 95−113) domains (Figure 2). The core domain consists of a five-stranded parallel β-sheet (S3, residues 59−65; S4, residues 82−88; S7, residues 122−128; S8, residues 141−156; and S9, residues 171−176). This core domain corresponds to the conserved type I PRTase fold (*12*, *13*) flanked by four α-helices, H3 and H4 (residues 36−53 and 68−79, respectively) located on one side of the β-sheet and H5 and H6 (residues 134−146 and 163−169, respectively) on the other side. The hood domain includes two α-helices (H1, residues 12−18; and H2, residues 30−35) and two β-strands (S1, residues 13−17; and S2, residues 24−29). In this AMP-containing hAPRT structure, the flexible loop is formed by two β-sheets (S5, residues 95−103; and S6, residues 106−113) folded in the open conformation. It was observed as a "calyx-like" feature, formed by the side chains of Phe16, Phe19, and Phe26 (Figure 3). This arrangement is located at the dimerization interface. The Pro93 side chain of the other monomer is positioned pointing toward the center of the calyx. A close inspection of this feature suggested that Pro96, Gly90, and Gly94 participate in stabilizing this structural organization. A search for similar structural conformations was performed using the SPASM web server (*32*) and none was identified, suggesting that such a side chain arrangement is uncommon and perhaps a feature that might be relevant.

Structural Comparisons and APRT Base Specificity. Several conserved residues of type I PRTases have been shown to be important for binding the nucleophile during a catalytic cycle. These include the hood subdomain of the known PRTases (*9*−*12*, *33*). Despite the structural variability among different PRTases, the hood contains one or two conserved residues. Those residues are responsible for determining either the purine or the pyrimidine nucleophile affinity of the enzyme. In addition, the hood subdomain contains a highly conserved aromatic residue involved in the correct positioning of the purine or pyrimidine base. In the AMP-bound hAPRT structure, the carbonyl oxygen of Val25 forms a hydrogen bond with the adenine N6 atom and the

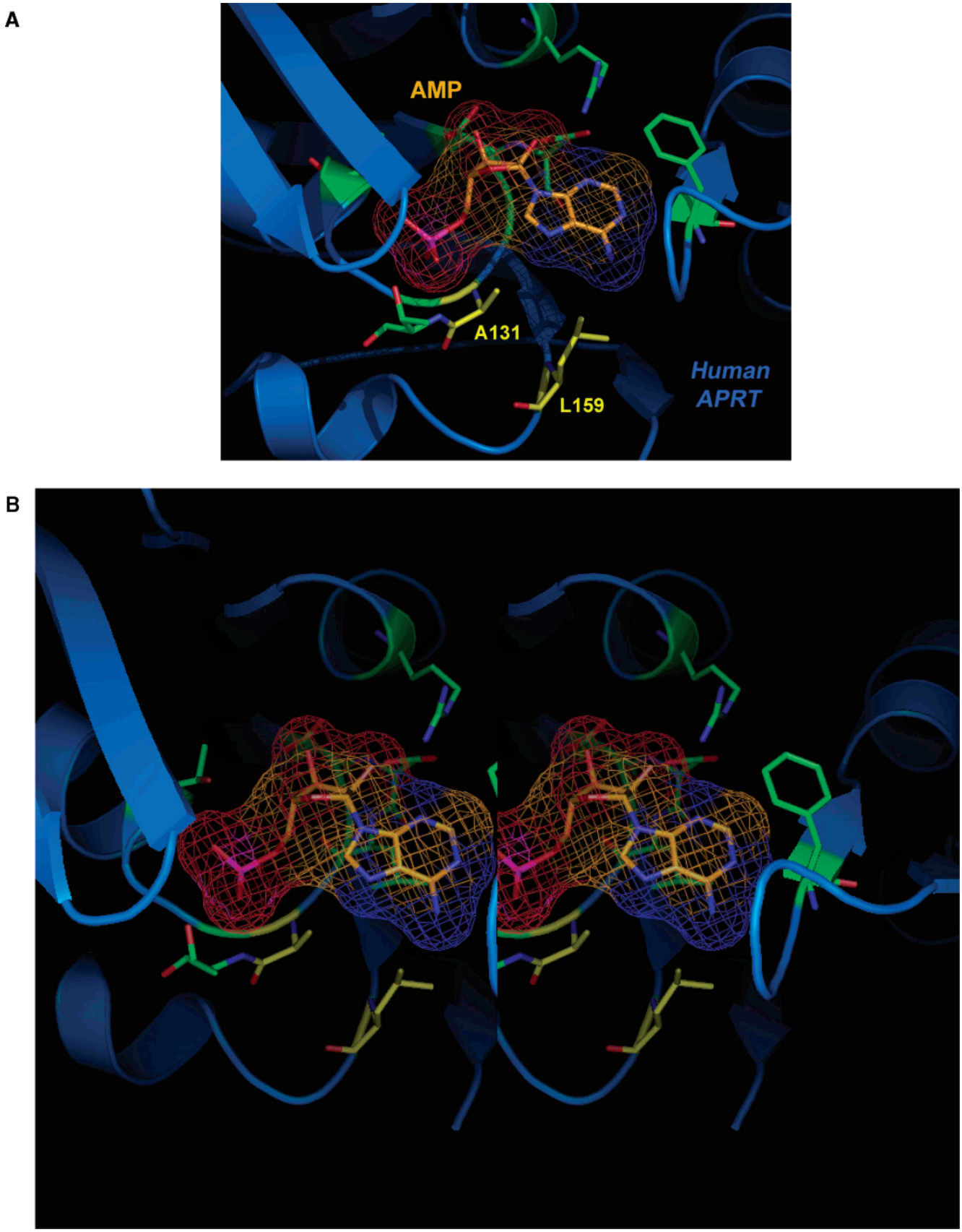

FIGURE 4: (A) Cartoon diagram of the AMP-bound hAPRT structure showing selected residues of the active site (carbon atoms in green) and AMP (carbon atoms in orange and surface in mesh). Ala131 and Leu159, which have been associated with base specificity, are shown with carbon atoms in yellow. (B) Stereoview of the detail of the hAPRT active site showing selected residues which interact with AMP.

Arg27 amide nitrogen forms a hydrogen bond with the adenine N1 atom. These contacts are equivalent to *S. cerevisiae* APRT−adenine contacts, which are formed by the Leu26 oxygen and Glu28 nitrogen atoms (*33*) with the base. In *L. tarentolae* APRT, Phe42 stacks against the purine base. In contrast, the corresponding atoms in the *Tr. cruzi*

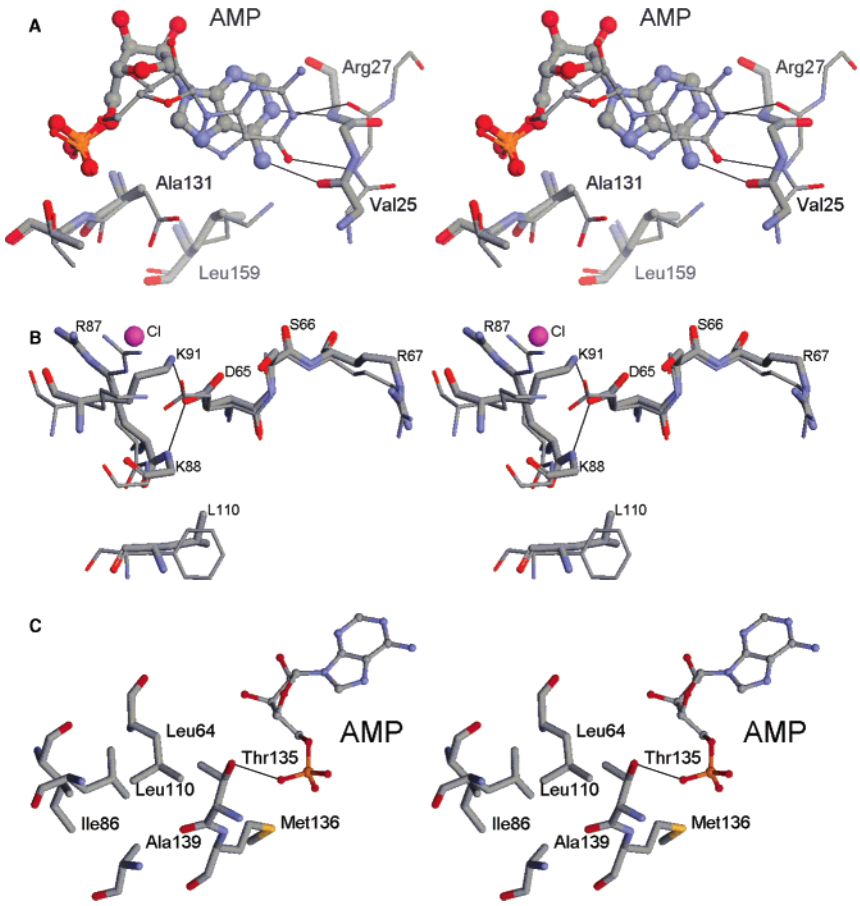

FIGURE 5: (A) Stereoview of the superposition of the hAPRT and human HGPRT active sites. It is likely that, in addition to the main chain contacts and π-stacking interaction originating from the hood subdomain side chains, the residues located at the positions corresponding to Leu159 and Ala131 in human APRT (residues labeled and shown as thick cylinders) explain the different specificities of type I PRTases for their respective bases. (B) Stereoviews of selected residues of superimposed hAPRT and *S. cerevisiae* APRT structures. In the AMP-bound hAPRT structure (residues labeled and shown as thick cylinders), the Asp65-Ser66-Arg67 segment is in the *cis* conformation and the Asp65 side chain forms hydrogen bonds (shown as lines) with the N_η backbone atom of *cis*-Lys88 as well as the Lys91 N_ζ atom. Arg87 does not contact Asp65, as opposed to the equivalent arginine residue in *S. cerevisiae* APRT, which forms a salt bridge with the aspartic residue. (C) Stereoview of selected residues of the hAPRT active site. Leu110 (conserved hydrophobic residue at this position) and Leu64 interact with the CG atom of Thr135, which is inserted in a hydrophobic environment formed by Ile86, Ala139, and Met136, orienting thus the hydroxyl group of this residue toward the 5′-phosphate moiety of PRPP (or AMP). In the AMP-bound human APRT structure, the hydroxyl group of Thr135 forms a hydrogen bond (shown as a line) to the phosphate moiety of AMP.

HGPRT structure in complex with the hypoxanthine analogue 7-hydroxy[4,3-*d*]pyrazolpyrimidine are the nitrogen and oxygen atoms of Val165 (*13*). These differences may have evolved to accommodate the carbonyl oxygen connected to the purine ring of hypoxanthine rather than the corresponding amino group attached to adenine (Figures 4 and 5A). Given this structural variability, the hood subdomain may not be sufficient for base specificity (*9*−*13*). On the basis of the hAPRT structure, we suggest that Leu159 and Ala131 might contribute to select adenine over different purines through hydrophobic interactions. In agreement with this hypothesis, Denessiouk and Johnson (*34*) identified a common structural framework for the adenine binding, incorporating both polar and hydrophobic interactions between the protein and the ligand. Similarly, Nobeli *et al*. (*35*) demonstrated that protein−adenine complexes exhibit hydrophobic interactions below and above the purine ring, stacked by arginine residues (*36*). Guanines on the other hand are less exposed to the solvent than adenines and interact with glutamic and aspartic acid residues (*36*).

In the hAPRT structure, the highly conserved Arg67 interacts with the adenine base. Moreover, PRTases that binds hypoxanthine, xanthine, or guanine present lysine residues in direct contact with guanine, which is located at the position equivalent to Leu159 of hAPRT. This position in adenine phosphoribosyltransferases is always occupied by a hydrophobic residue, either isoleucine or leucine (*33*, *37*, *38*). Interestingly, a single residue change (Lys134Ser) in *Tri. foetus* HGXPRT enables it to bind adenine (*12*). The hydrophobic Ala131 residue observed in the hAPRT structure is highly conserved across APRTases (*33*). In *T. gondii* UPRT, an alanine residue is observed in the equivalent position and all known OPRTase structures contain a threonine residue in the equivalent position (*36*, *39*, *40*). In contrast, PRTases that bind hypoxanthine, xanthine, or guanine bases have aspartic acid residues located at the equivalent position, in direct contact with the bases (*5*, *6*, *12*, *13*, *34*, *35*). Thus, it is likely that, in addition to the main chain contacts and π-stacking interaction, the residues located at the positions corresponding to Leu159 and Ala131 in hAPRT explain the base specificities of type I PRTases as shown in Figures 4 and 5A.

Human APRT Structure−*Function Relationship with Clinically Important Mutations.* Human APRT deficiency leads

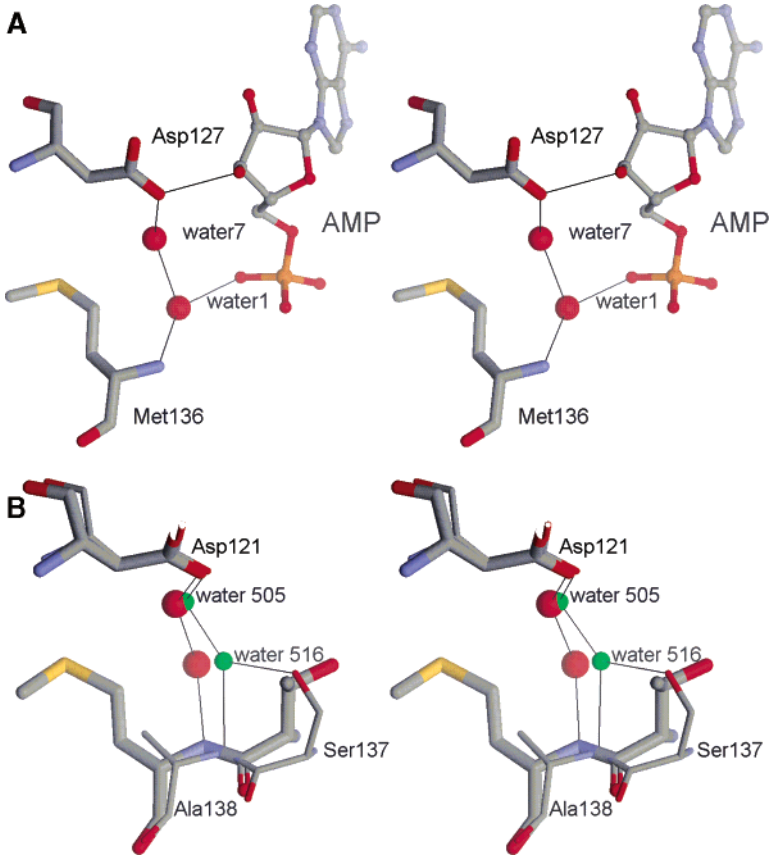

FIGURE 6: (A) Stereoview of selected residues and water molecules of the hAPRT active site. In the human APRT structure, the water1 and water7 molecules participate in a hydrogen bond network (shown as lines) involving especially the 5′-phosphate moiety of PRPP (or AMP), the Met136 backbone nitrogen, and a δ-oxygen atom of the conserved Asp127 residue. Water1 must be an important element for PRPP binding, and perhaps the Met136Thr mutation favors competition of the hydroxyl group with the backbone nitrogen atom of the same Thr136 residue for this water, shifting this molecule closer to the threonine residue and, consequently, disfavoring the bond to the 5′-phosphate group. (B) Stereoview of selected residues and water molecules of superimposed hAPRT and *S. cerevisiae* APRT structures. In the *S. cerevisiae* APRT structure (residues labeled and shown as thick cylinders), which does not contain either a PRPP or a AMP bound, the equivalent water 516 (water1 in hAPRT) forms a hydrogen bond to Ser137 (Thr135 in hAPRT) and, as opposed to water505 (water7 in hAPRT), is shifted compared to the positions of the equivalent waters of the three other structures, which bind PRPP or AMP. All the hydrogen bonds are shown as lines.

to an increase in the level of adenine oxidation by xanthine oxidase, resulting in the accumulation of 2,8-dihydroxyadenine (DHA), an insoluble compound the accumulation of which causes urolithiasis and kidney failure. At least seven missense mutations and one deletion in hAPRT are associated with such renal dysfunction (*17*, *33*). The known hAPRT mutations cluster into three regions: the one that binds to the PRPP β-phosphate group, the one that binds to the PRPP 5′-phosphate group, and the region of the flexible loop that is proposed to close the active site during catalysis (*9*).

The Asp65Val (*41*) mutation is close to the PRPP β-phosphate binding site. Phillips *et al.* (*10*) observed that the carboxylate group of the equivalent *L. donovani* Asp80 forms hydrogen bonds with the N_ϵ and $N_{\eta 2}$ atoms of the conserved Arg102. This residue, Arg102, contacts the other APRT monomer of the dimer, at the PRPP β-phosphate group. The same Asp80 side chain hydrogen bonds the N_η backbone atom of *cis*-Ala81, thereby stabilizing, with these two interactions, the unusual *cis*-peptide conformation of the Glu61-Ser62-Arg63 segment. This *cis*-peptide sequence is thought to be conserved in all APRTases and to be essential to PRPP pyrophosphate binding (*9*). *trans*- and *cis*-peptide conformations of this segment (Glu61-Ser62-Arg63) have been observed in high-resolution crystal structures of type I PRTases when the pyrophosphate binding site is empty (*9*). Nevertheless, the *trans* conformation has never been detected when PRPP is bound to the active site (*11*, *12*, *36*). In the human APRT structure, the Asp65-Ser66-Arg67 segment is in the *cis* conformation and the Asp65 side chain forms hydrogen bonds with the N_η backbone atom of *cis*-Lys88, as well as with the conserved basic residue Lys91 N_ζ atom (Figure 5B) (*33*). Arg87 (Arg89 in *S. cerevisiae* APRT) does not contact the aspartic acid residue, reinforcing the importance of the *cis* conformation for binding the pyrophosphate of PRPP (Figure 5B). The Asp65Val mutation is likely to enable a shift of the valine residue close to Leu110, a position always occupied by a hydrophobic residue in al APRTases. Such positioning will allow the Val65-Ser66-Arg67 segment to adopt the *trans* conformation, preventing PRPP binding.

The Leu110Pro (*42*) mutation is associated with renal dysfunction in humans. Inspection of the human APRT structure does not clearly reveal the correlation of the Leu110Pro mutation with APRT activity and therefore clinical dysfunction (*10*). However, Leu110 is a conserved hydrophobic residue, and Leu64 interacts with the CG atom of Thr135 (Figure 5C). Thr135 is inserted in a hydrophobic environment formed by Ile86, Ala139, and Met136, thus orienting the hydroxyl group of Thr135 toward the 5′-phosphate moiety of PRPP (or AMP). In the human APRT structure, the hydroxyl group of Thr135 forms hydrogen

bonds with the phosphate moiety of AMP (see Figure 5C). On the basis of the rotamer database of O, Thr135 can adopt three rotamer conformations, of which only one has its hydroxyl group oriented toward the 5′-phosphate. We hypothesize that the other two possible rotamers of Thr135 are disfavored in the presence of the neighboring Leu110. The Leu110Pro mutation at this position could favor the other rotamer conformations and allow the γ-carbon of Thr135 to point to the 5′-phosphate binding site, obstructing PRPP from binding to the active site and hence compromising APRT function.

A third and very common human APRT mutation, Met136Thr (*43*), is localized in the 5′-phosphate binding loop. In hAPRT, Met136 is in a closely packed environment, similar to the equivalent residue Ala155 from the *L. donovani* homologue (*10*). Comparable arrangements are also observed in the *G. lamblia* and *S. cerevisiae* APRT structures (*9*, *33*). Philips *et al*. (*10*) suggested that the substitution of Met136 with the β-branched threonine side chain could disrupt the conformation of the Ala131−Thr135 segment at the PRPP-binding motif. Superimposing the hAPRT structure with the other known APRT structures has identified two water molecules whose positions are highly conserved in all APRTases. In the hAPRT structure, these water molecules (water1 and water7, Figure 6A) participate in a hydrogen bond network involving the 5′-phosphate moiety of PRPP (or AMP), the Met136 nitrogen backbone, and a δ-oxygen atom of the conserved Asp127 residue (Figure 6A). We predict that water1 must be an important element for PRPP binding and therefore propose that the Met136Thr mutation (*43*) favors the competition of the hydroxyl group of water1 with the Thr136 backbone nitrogen, shifting water1 toward the Thr136 residue. This change in the position of water1 hampers its binding to the 5′-phosphate group and results in a reduced activity of Met136Thr APRT. *G. lamblia* and *S. cerevisiae* APRT structures have a γ-branched leucine and an alanine residue, respectively (*9*, *33*), at the position equivalent to Met136 of human APRT. The conformation of the 5′-phosphate binding loop in both cases is very similar. Interestingly, in the *S. cerevisiae* APRT structure (*33*), which does not have either PRPP nor AMP bound, the equivalent to water1 of hAPRT is water516, which hydrogen bonds to Ser137, which is equivalent to Thr135 of hAPRT. Also, water505 of the *S. cerevisiae* enzyme, equivalent to water7 of hAPRT, is shifted compared to the position of the equivalent water of the other known APRT structures (Figure 6B). Our proposed interference with the mechanism of the Met136Thr mutation is supported by the modest (10.3%) loss of activity described for such a mutation in the human APRT (*43*).

SUMMARY AND CONCLUSIONS

The atomic structure of the human APRT (hAPRT) in complex with AMP at 2.1 Å resolution has been determined, representing the first human type I PRTase structure that has been resolved. Structural comparisons of hAPRT with other PRTases whose structures have been determined reveal details from which it was possible to propose that the residues located at positions corresponding to Leu159 and Ala131 in hAPRT are responsible for the base specificities of type I PRTases. Three missense mutations in hAPRT associated with serious renal dysfunctions have been analyzed on the basis of our data and other known APRT structures. A novel finding is the assignment of function to those three point mutations, identified as being responsible for DHA-urolithiasis and renal failure. From such studies, we predict that water1 is an important element for PRPP binding. The Asp65Val mutation is likely to enable a shift of the valine residue close to Leu110, a position always occupied by a hydrophobic residue in all APRTases. Such positioning will allow the Val65-Ser66-Arg67 segment to adopt the *trans* conformation, preventing PRPP binding. We also propose that the Met136Thr mutation favors the competition of the hydroxyl group of water1 with the backbone nitrogen of Thr136, shifting water1 toward the Thr136 residue. This change in the position of water1 will disfavor its binding to the 5′-phosphate group and will result in a reduced APRT activity of Met136Thr. Additionally, Leu110, a conserved hydrophobic residue, contributes, via its interaction with the CG atom of Thr137, to the orientation of the hydroxyl group of this residue toward the 5′-phosphate moiety of PRPP (or AMP) in APRTases.

ACKNOWLEDGMENT

We thank the members of the Protein Crystallography and Structural Biology Group (IFSC-USP) for the helpful discussions during the course of this work. We are grateful to Dr. Prof. Lewis J. Greene and Dr. Victor M. Faça of the Protein Chemistry Center, Medicine School of Ribeirão Preto, for the hAPRT N-terminal sequencing.

REFERENCES

1. Simmonds, H. A., Sahota, A., and Acker, K. J. V. (1995) in *The Metabolic and Molecular Bases of Inherited Disease* (Stanbury, J. B., Wyngaarden, J. B., and Fredrickso, D. G., Eds.) McGraw-Hill, New York.
2. Engle, S. J., Stockelman, M. G., Chen, J., Boivin, G., Yum, M. N., Davies, P. M., Ying, M. Y., Sahota, A., Simmonds, H. A., Stambrook, P. J., and Tischfield, J. A. (1996) Phosphoribosyltransferase-deficient mice develop 2,8-dihydroxyadenine nephrolithiasis, *Proc. Natl. Acad. Sci. U.S.A. 93*, 5307−5312.
3. Williams-Ashman, H. G., Seidenfeld, J., and Galletti, P. (1982) Trends in the biochemical pharmacology of 5′-deoxy-5′-methylthioadenosine, *Biochem. Pharmacol. 31*, 277−288.
4. Greenwood, M. C., Dillon, M. J., Simmonds, H. A., Barratt, T. M., Pincott, J. R., and Metreweli, C. (1982) Renal failure due to 2,8-dihydroxyadenine urolithiasis, *Eur. J. Pediatr. 138*, 346−349.
5. Kamatani, N., Hakoda, M., Otsuka, S., Yoshikawa, H., and Kashiwazaki, S. (1992) Only three mutations account for almost all defective alleles causing adenine phosphoribosyltransferase deficiency in Japanese patients, *J. Clin. Invest. 90*, 130−136.
6. Stone, T. W., and Simmonds, H. A. (1991) in *Purines: Basic and Clinical Aspects* (Kluwer, Ed.) Academic Press, London.
7. Wyngaarden, J. B., and Dunn, J. T. (1957) 8-Hydroxyadenine as the Intermediate in the Oxidation of Adenine to 2,8-Dihydroxyadenine by Xanthine Oxidase, *Arch. Biochem. Biophys. 70*, 150−156.
8. De Vries, A., and Sperling, O. (1977) Implications of disorders of purine metabolism for the kidney and the urinary tract, *Ciba Found. Symp. 48*, 179−206.
9. Shi, W., Sarver, A. E., Wang, C. C., Tanaka, K. S. E., Almo, S. C., and Schramm, V. L. (2002) Closed Site Complexes of Adenine Phosphoribosyltransferase from *Giardia lamblia* Reveal a Mechanism of Ribosyl Migration, *J. Biol. Chem. 277*, 39981−39988.
10. Phillips, C. L., Ullman, B., Brennan, R. G., and Hill, P. C. (1999) Crystal structures of adenine phosphoribosyltransferase from *Leishmania donovani*, *EMBO J. 18*, 3533−3545.
11. Focia, P. J., Craig, S. P., and Eakin, A. E. A. (1998) Approaching the transition state in the crystal structure of a phosphoribosyltransferase, *Biochemistry 37*, 17120−17127.
12. Vos, S., Parry, R. J., Burns, M. R., de Jersey, J., and Martin, J. L. (1998) Structures of Free and Complexed Forms of *Escherichia*

coli Xanthine-Guanine Phosphoribosyltransferase, *J. Mol. Biol. 282*, 875−889.
13. Shi, W., Li, C. M., Tyler, P. C., Furneaux, R. H., Grubmeyer, C., Schramm, V. L., and Almo, S. C. (1999) The 2.0 Å Structure of Human Hypoxanthine-Guanine Phosphoribosyltransferase in Complex with a Transition State Inhibitor, *Nat. Struct. Biol. 6*, 588−593.
14. Vogelstein, B., and Gillespie, D. (1979) Preparative and analytical purification of DNA from agarose, *Proc. Natl. Acad. Sci. U.S.A. 76* (2), 615−619.
15. Ausubel, F. M., Brent, R., Kingston, R. E., Moore, D. D., Seidman, J. G., Smith, J. A., and Struhl, K. (1995) in *Short Protocols in Molecular Biology*, John Wiley & Sons, New York.
16. Tuttle, J. V., and Krenitsky, T. A. (1980) Purine phosphoribosyltransferases from *Leishmania donovani*, *J. Biol. Chem. 255*, 909−916.
17. Del Sol, F. G., RamoÂn-Maiques, S., Santos, C. F., Grangeiro, T. B., Nagano, C. S., Farias, C. M. S. A., Cavada, B. S., and Calvete, J. J. (2002) Crystallization and preliminary X-ray diffraction analysis of the seed lectin from *Parkia platycephala*, *Acta Crystallogr. D58*, 167−169.
18. Chang, G., and Lewis, M. (1994) The *CCP*4 suite: programs for protein crystallography, *Acta Crystallogr. D50*, 760−763.
19. Navaza, J. (1994) *AMoRe*: an automated package for molecular replacement, *Acta Crystallogr. A50*, 157−163.
20. Silva, M., Silva, C. H. T. P., Iulek, J., Oliva, G., and Thiemann, O. H. (2004) Crystal structure of adenine phosphoribosyltransferase from *Leishmania tarentolae*: potential implications for APRT catalytic mechanism, *Biochim. Biophys. Acta* (in press).
21. Brunger, A. T., Adams, P. D., Clore, G. M., Delano, W. L., Gros, P., Grosse-Kunstleve, R. W., Jiang, J. S., Kuszewski, J., Nilges, N., Pannu, N. S., Read, R. J., Rice, L. M., Simonson, T., and Warren, G. L. (1998) Crystallography & NMR System: A New Software Suite for Macromolecular Structure Determination, *Acta Crystallogr. 54*, 905−921.
22. Murshudov, G. N., Vagin, A. A., and Dodson, E. J. (1997) Refinement of Macromolecular Structures by the Maximum-Likelihood Method, *Acta Crystallogr. 53*, 240−255.
23. McRee, D. E. (1992) A Visual Protein Crystallographic Software System for X11/Xview, *J. Mol. Graphics 10*, 44−46.
24. Perrakis, A., Morris, R. J. H., and Lamzin, V. S. (1999) Automated protein model building combined with iterative structure refinement, *Nat. Struct. Biol. 6*, 458−463.
25. Jones, T. A., Zon, J. Y., Cowan, S. W., and Kjelgaard, M. (1991) Improved methods for building protein models in electron density maps and the location of errors in these models, *Acta Crystallogr. A47*, 110−119.
26. Appel, R. D., Bairoch, A., and Hochstrasser, D. F. (1994) A new generation of information retrieval tools for biologists: the example of the ExPASy WWW server, *Trends Biochem. Sci. 19*, 258−260.
27. Thomas, C. B., Arnold, W. J., and Kellyey, W. N. (1973) Human Adenine Phosphoribosyltransferase. Purification, subunit structure, and substrate specificity, *J. Biol. Chem. 248*, 2529−2535.
28. Holden, J. A., Meredith, G. S., and Kelley, W. N. (1979) Human adenine phosphoribosyltransferase. Affinity purification, subunit structure, amino acid composition, and peptide mapping, *J. Biol. Chem. 254*, 6951−6955.
29. Okoda, G., Kaneko, I., and Koyama, H. (1986). Purification and characterization of adenine phosphoribosyltransferase from mouse mammary carcinoma FM3A cells in culture, *Biochim. Biophys. Acta 884*, 304−310.
30. Nayal, M., and Di Cera, E. (1996) Valence Screening of Water in Protein Crystals Reveals Potential Na^+ Binding Sites, *J. Mol. Biol. 256*, 228−234.
31. Kleywegt, G. J., Zou, J. Y., Kjeldgaard, M., and Jones, T. A. (2001) in *International Table for Crystallography* (Rossmann, M. G., and Arnold, E., Eds.) pp 353−356, Kluwer Academic Publishers, Dordrecht, The Netherlands.
32. Kleywegt, G. J. (1999) Recognition of spatial motifs in protein structures, *J. Mol. Biol. 285*, 1887−1897.
33. Shi, W., Tanaka, K. S. E., Crother, T. R., Taylor, M. W., Almo, S. C., and Schramm, V. L. (2001) Structural Analysis of Adenine Phosphoribosyltransferase from *Saccharomyces cerevisiae*, *Biochemistry 40*, 10800−10809.
34. Denessiouk, K. A., and Johnson, M. S. (2000) A common structural framework for adenine and AMP binding in 13 unrelated protein families, *Proteins: Struct., Funct., Genet. 38*, 310−326.
35. Nobeli, I., Laskowski, R. A., Valdar, W. S. J., and Thornton, J. M. (2001) On the molecular discrimination between adenine and guanine in proteins, *Nucleic Acids Res. 29*, 4294−4309.
36. Scapin, G., Ozturk, D. H., Grubmeyer, C., and Sacchettini, J. C. (1995) The Crystal Structure of the Orotate Phosphoribosyltransferase Complexed with Orotate and α-D-5-Phosphoribosyl-1-pyrophosphate, *Biochemistry 34*, 10744−10754.
37. Eads, J. C., Scapin, G., Xu, Y., Grubmeyer, C., and Sacchettini, J. C. (1994) The crystal structure of human hypoxanthine-guanine phosphoribosyltransferase with bound GMP, *Cell 78*, 325−334.
38. Somoza, J. R., Chin, M. S., Focia, P. J., Wang, C. C., and Fletterick, R. J. (1996) Crystal Structure of the Hypoxanthine-Guanine-Xanthine Phosphoribosyltransferase from the Protozoan Parasite *Tritrichomonas foetus*, *Biochemistry 35*, 7032−7040.
39. Henriksen, A., Aghajari, N., Jensen, K. F., and Galhede, M. (1996) A Flexible Loop at the Dimer Interface is a Part of the Active Site of the Adjacent Monomer of *Escherichia coli* Orotate Phosphoribosyltransferase, *Biochemistry 35*, 3803−3809.
40. Schumacher, M. A., Carter, D., Scott, D. M., Roos, D. S., Ullman, B., and Brennan, R. G. (1998) Crystal structures of *Toxoplasma gondii* uracil phosphoribosyltransferase reveal the atomic structure of pyrimidine discrimination and prodrug binding, *EMBO J. 18*, 3219−3232.
41. Chen, J., Sahota, A., Laxdal, T., Stambrook, P. J., and Tischfield, J. A. (1990) Demonstration of a common mutation at the adenine phosphoribosyltransferase (APRT) locus in the Icelandic population, *Am. J. Hum. Genet. 47* (Suppl.), A152.
42. Sahota, A., Chen, J., Boyadijev, S. A., Gault, M. H., and Tischfield, J. A. (1994) Missense mutation in the adenine phosphoribosyltransferase gene causing 2,8-dihydroxyadenine urolithiasis, *Hum. Mol. Genet. 3*, 817−818.
43. Hidaka, Y., Tarle, S. A., Fujimori, S., Kamatani, N., Kelley, W. N., and Palella, T. D. (1988) Human adenine phosphoribosyltransferase deficiency. Demonstration of a single mutant allele common to the Japanese, *J. Clin. Invest. 81*, 945−950.

BI0360758